Density functional studies of protonated and alkali metal (Li, Na and K) incorporated T-doped 2D zeolite model (T= B, Ga)

N.F. Andriambelaza[a,*], C. Perry[b], J. Mugo[b], M. Sarwar[c], G. Jones[c], N. Chetty[d]

[a]*Department of Physics, University of Pretoria, Pretoria 0002, South Africa*
[b]*Johnson Matthey Technology Centre, Billingham, Cleveland, TS23 1LB, UK*
[c]*Johnson Matthey Technology Center, ReadingRG4 9NH, U.K.*
[d]*Faculty of Science, University of Witwatersrand, Johannesburg 2000, South Africa*

Abstract

Ab initio calculations based on density functional theory (DFT) have been performed to investigate the role of trivalent atoms substituting silicon atom in the 2D zeolite model. The effects of the B and Ga atoms on the stability, structural and electronic properties of the 2D zeolite model are explored. Our DFT calculations reveal that the introduction of B atom is exothermic whereas that one of Ga atom is endothermic. The structural analysis shows that the incorporation of B and Ga atoms affects the bond lengths of the system, however it does not lead to a significant deformation of the structure. The Fermi level of the doped systems is shifted towards the valence band, indicating that the incorporation of these trivalent atoms leads to $p-$type materials. The second purpose of this study is to find the suitable charge compensations among hydrogen and alkali metals as well as their site preference (either on the surface or in the cages of the silica bilayer). The calculated formation energy values are similar, suggesting both configurations could co-exist. Hydrogen has the lowest formation energy and the proton affinity analysis predicts low acid strength of H-B- compared to H-Ga-doped 2D zeolite, a similar trend to that of bulk zeolite. Among the alkali elements, we found that Na and K atoms are the most stable ones. The density of states analysis shows that the Fermi level is lying within the gap, and defect states are observed near the band edges narrowing the band gap of the system. This work provides detailed and valuable information about the atomic-level properties of the relatively recent 2D zeolite model, which is beneficial for its industrial applications.

1. Introduction

Zeolites are generally known as microporous crystalline aluminosilicate materials constituted by the primary building blocks SiO_4 and AlO_4 tetrahedra. The latter interconnect each other to form cavities of different shapes and sizes. The presence of these cavities allows the zeolites to adsorb molecules and ions [1, 2, 3], and also to be used in separation processes as molecular sieves [4, 5]. The presence of Al atoms in the framework results in a net negative charge to the framework, which is normally compensated by a proton or a cation, most commonly alkali metals and alkaline earth ions. The presence of these extra-cations inside the cavities makes the zeolites promising materials for ion exchange. Due to these unique properties, the zeolite materials have been widely used for water purification in order to remove ammonia and heavy metals from industrial and drinking water [6, 7]. Furthermore, the cations can also effectively serve as adsorption sites [8] or as a Brønsted acid site in the case of a proton. These characteristics are important for catalysis applications. The location of these cations has been subject of many theoretical and experimental work as it defines the efficiency of the zeolite materials. For instance, Civalleri *et al.* [9] performed ab initio calculations to investigate the site preference and the relative stability of H, Li, Na, and K in Al-substituted silica zeolite called chabazite. Li and Na atoms were found to be more stable at the 6-membered ring

*Corresponding author
Email address: arinala.f@gmail.com (N.F. Andriambelaza)

whereas K prefers the 8-membered ring site. The H atom forms a hydroxyl group with the O atom that has dangling bond due to the introduction of the Al atom. The latter is the initial and the most popular trivalent atom known to induce catalytically active sites in zeolites. However, much attention has been devoted to the synthesis and characterization of other trivalent atoms such as B, Ga and Fe to tailor the physicochemical properties of the zeolites. In his experimental work, Chu [10] performed infrared spectroscopy and temperature-programmed desorption to study the acidity of T-doped ZSM5 (M = B, Ga, Fe). The properties of B-, Al-, Ga-, and Fe-substituted zeolites have also been investigated theoreticallly using DFT method [11, 12]. The experimental and theoretical results agreed that these substitution defects are stable and the relative acidic order of the substituted zeolite usually has the order B < Fe < Ga < Al.

In the past, zeolites were perceived as covalently bonded continuous frameworks in three dimensions. Some challenges were encountered for the study of these 3D zeolites such as diffusion issues, limited accessibility for larger molecules, and challenges in synthesis. These limitations led to the development of two dimensional (2D) zeolites, which offer improved molecular access, enhanced catalytic performance, and simpler synthesis routes, addressing many of the constraints of their 3D counterparts. Actually, 2D materials in general have demonstrated potential owing to their distinctive physical and chemical properties. Recent researches reveal that 2D materials serve as effective catalysts for carbon dioxide reduction, achieving remarkable Faradaic efficiency and improved conversion rates [13]. Mao et al. [14] investigated that molybdenum disulfide can also serve as an effective catalyst for the oxygen reduction reaction (ORR). It was also reported that 2D materials are highly effective for oxygen evolution reaction (OER) applications because of their numerous advantages, including a large surface-to-bulk ratio and increased exposure efficiency of catalytic active sites[15]. These represent only a small subset of the wide-ranging applications of 2D materials. Several 2D zeolites have been successfully synthesized using different techniques such as MFI, FAU, MOR, MWW, TS-1, and have been used effectively as catalysts in the various reactions. For instance, Choi *et al*. [16] developed nanosheets of MFI using appropriately designed bi-functional surfactants. The catalytic performance of these MFI nanosheets was investigated by cracking a large organic molecule known as polyethylene. They reported that these nanosheets exhibits interesting catalytic activity due to a large number of acid sites located at the mesopore surface. They also tested the durability of the catalytic lifetime of these MFI zeolites in methanol-to-gasoline conversion. An important durability was noticed compared to conventional zeolite making them highly efficient for industrial catalytic applications. These findings were also confirmed by a work carried by Wei *et al*. [17], who compared the catalytic performance of 2D versus 3D MFI zeolite in three selected liquid phase reactions. They found that that the 2D samples demonstrated much higher catalytic activity and resistance to deactivation. It is important to highlight that the 2D zeolites listed above mirror an existing 3D zeolites.

In recent years, an alternative model of 2D zeolites was proposed by Boscoboinik *et al*. [18, 19]. They demonstrated that 2D bilayer silica material can be an effective model for 2D zeolite. The surfaces of this 2D material do not have any dangling bonds which model well the feature of the interior of the zeolite pores. To validate this model, Boscoboinik *et al*. [18, 19] conducted an experiment where they substituted one Si atoms of the bilayer with an Al atom. They found that the Al atoms prefer to substitute the Si atom on top layer, and the dangling bonds at O atoms due the Al substitution can be compensated by a proton originated from water adsorption. The O−H bridge formed shows strong acidity upon adsorption of CO molecules. Furthermore, a H and D exchange was observed upon D_2O adsorption. The properties of this bridging hydroxyl correspond well to what is found in regular zeolites. Various studies have been done [18, 19, 20, 21] and research is ongoing on Al-substituted silica bilayer. However, the investigation can also extend beyond conventional Al doping. That is, our work introduces boron and gallium as novel dopants in the 2D zeolite, offering a new pathway to modulate acidity and enhance

catalytic performance, thus expanding the functional versatility of zeolite-based catalysts. To the best of our knowledge, this approach has not been explored previously. In the present manuscript, the roles of B and Ga atoms substituting one Si atom of the silica bilayer are investigated and compared. The effects of these trivalent atoms on the stability, structural and electronic properties of the 2D zeolite model are scrutinized. The second purpose of this study is to find the site preference of the extra-cations such as hydrogen and alkali metals (Li, Na, and K). The stability of the various configurations are evaluated by calculating the formation energy. Further, a detailed understanding of the structural and electronic properties as well as the chemical interactions taking place between the 2D silicate framework atoms and the foreign atom is very important for the applications. That is, an extensive theoretical study of these properties mentioned above is carried out in the last part of this manuscript.

2. Computational details

First-principles calculations using DFT approaches as implemented in Quantum Espresso software [22, 23] are performed. Spin polarized calculations using generalized gradient approximation (GGA) with the Perdew-Burke-Ernzerhof (PBE) [24] parameterization is used as exchange-correlation functional. The core-electrons interactions are described by projector augmented wave (PAW) method [25]. In all calculations, Van der Waals interactions are considered using vdw-DF2 approximation [26, 27, 28]. A vacuum layer of 15 Å is considered to isolate the bilayer. A test of convergence of the cutoff was carried out by varying its value from 10 to 90 Ry with a step increase of 10 Ry. We observed that the energy of the relaxed structure only changes less than 10^{-3} Ry above 50Ry. Therefore, in this study a cutoff energy of 50Ry was considered. For the Brillouin zone sampling, $4 \times 4 \times 1$ k-mesh are used. The relaxation convergence of energy is taken as 10^{-6} eV and the Hellmann-Feynman force between each atom set to less than 0.001 eV/Å.

3. Results and discussion

3.1. Pristine 2D zeolite material: structural and electronic properties

The 2D zeolite model is composed by superposition of two tetrahedra SiO_4 (see Fig. 1) which, in total, forms five layers of atoms: three layers of O atoms and two layers of Si atoms. The two layers of O atoms on top and bottom of the bilayer act as bridges connecting the Si atoms on the same layer while the third one is found at the middle of the bilayer structure, joining the Si atoms for different layers. The top view of the structure

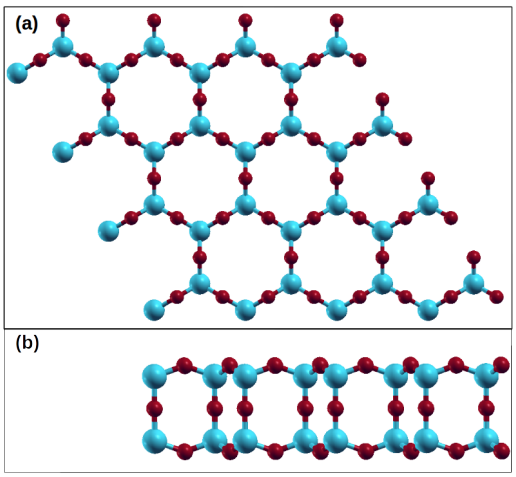

Figure 1: Atomic structure of the 2D zeolite model viewed from (a) top, (b) side. The blue and red spheres represent silicon and oxygen atoms, respectively.

presented in Fig. 1(a) clearly shows that this model has a hexagonal graphene-like structure (in zeolite terms, it is known as 6 membered-rings). From the side view shown in Fig. 1(b), a 4 membered-ring feature is observed. One important characteristic of the present silica bilayer structure is that all bonds are saturated validating the choice of this material as a model for 2D zeolite. This structure has a bond length (Si - O distance) of 1.63 Å which is consistent with that of bulk zeolite materials [29], and an interlayer, equivalent to Si - Si distance along the vertical, of z =4.35 Å.

To examine the electronic properties of the pristine 2D zeolite, total density of states (DOS) are plotted as shown in Figs. 2(a, b). The obtained plot shows that the pristine silica bilayer is a bandgap material with a large band gap value of 5.1 Å.

Spin polarized calculations were carried out to investigate the magnetic properties of the pristine material. It is observed that the DOS plots for the spin up and spin down are aligned to each other (see in Fig. 2(a, b)), indicating that this 2D zeolite model is a non-magnetic material. Next, the electronic structure of

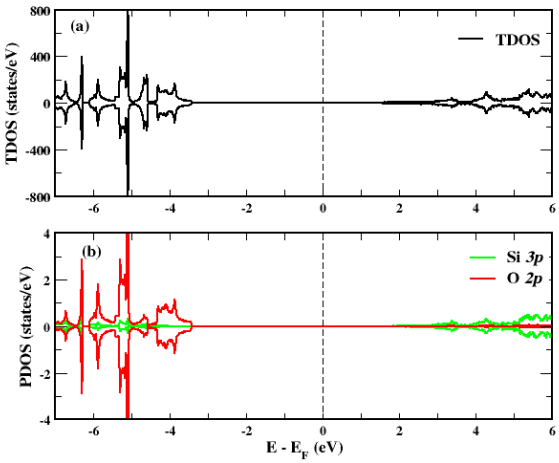

Figure 2: (a) Total and (b) partial density of states for the pristine 2D zeolite model. The black dashed vertical lines indicate the Fermi level.

an insulator/semiconductor is known to depend greatly on the contribution of the various orbitals at the band edges. Thus, we plotted the projected density of states (PDOS) of the pristine in Fig. 2(b). It is found that the valence band maximum (VBM) is composed mainly by the *p*-orbital of the O atom whereas the conduction band minimum (CBM) is populated by the *p*-orbital of the Si atom. Our results is consistent with previous study on bilayer material [30], as well as the orbital contributions at the band edges reported in the 3D bulk zeolite [31].

3.2. T-doped 2D zeolite (T = B, Ga)

In this section, substitution of one Si atom of the 2D zeolite framework with trivalent atoms such as B and Ga is investigated. The 2D zeolite model was prepared on a metallic substrate as a film [18, 19]. However, its interaction with the metallic substrate is weak, therefore, in this work freestanding bilayer of silica is considered for all calculations. It implies that all Si atoms in the 6-membered ring at the bottom and top layers of the bilayer structure are equivalent, and any Si atom in the supercell can be considered for the substitution. A large super-

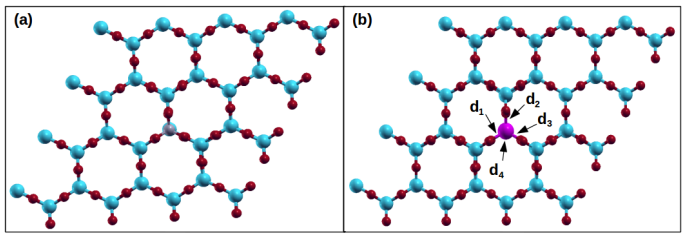

Figure 3: Top structures of single (a) B and (b) Ga-doped 2D zeolite. The blue, red, grey and magenta spheres are the Si, O, B and Ga atoms, respectively.

cell of 5 × 5 are considered to remove the interaction between the defect and its periodic images. The relaxed structures of B- and Ga-doped systems are shown in Fig. 3.

3.2.1. Structural properties

We firstly examine the structural properties of the trivalents incorporated silica bilayer. The values of various bond lengths in the system are summarized in Table 1. As displayed in Fig. 3, the parameters d_1, d_2 and d_3 depicted in Table 1 correspond to the bond lengths between the trivalent atoms and the three surrounding oxygens on the surface of the bilayer, while d_4 represents the distance between the trivalent atom and the oxygen at the middle of the bilayer structure. We observed that the B-O bonds are shorter than Si-O bonds in pure SiO_2 silica bilayer, as B atom has a smaller ionic radius and higher electronegativity compared to Si. In contrast, Ga atom has large ionic radius and low electronegativety leading to longer Ga-O bonds com-

Table 1: Relevant bond lengths in Å and substitution energy (eV) for trivalent atoms (B, Ga) doped 2D zeolite. d_{ref} represents the average length of T-O bond from literature

.

	d_1	d_2	d_3	d_4	d_{ref}	E_{sub}
B	1.50	1.50	1.50	1.44	1.38[a,b]	-11.65
Al	1.74	1.74	1.74	1.75	1.72[a], 1.71[c]	-9.74
Ga	1.86	1.86	1.86	1.85	1.75[a], 1.81[b]	6.96

[a]Ref [12], [b]Ref [11], [c]Ref [32]

pared to Si-O bonds. The measured T − O bond lengths in the 2D zeolite model are consistent with those of bulk zeolites and MFI nanosheets (see Table 1). Although the trivalent atom substitution slightly alters the bond length, it does not cause major structural deformation. This is supported by the top view of the T-doped relaxed structures in Fig. 3 where the graphene-like shape of the material is retained for both case, larger and smaller atomic radius trivalent atom substitution. This finding can tell us that the B and Ga atoms substitution in silica bilayer could be stable replacing Si atom. To confirm the stability of the trivalent atoms doped bilayer SiO_2, we investigate their subtitution energies in the next section.

3.2.2. Thermodynamic stability

To gain more information on the thermodynamic stability of the monodoped bilayer system, we evaluate the substitution energy based on the following reaction:

$$n\mathrm{SiO_2}\ (b) + \frac{1}{2}\mathrm{T_2O_3}\ (c) + \frac{1}{2}\mathrm{O_2}\ (m) \longrightarrow \mathrm{Si_{n-1}TO_{2n}}\ (b) + \mathrm{SiO_2}\ (q). \tag{1}$$

where T = (B, Ga) and n is the number of tetrahedra in the system. The letter in between brackets corresponds to the type of structure of each elements: b indicates a bilayer, c the corundum structure, q the α-quartz structure and m molecule. According to this equation, the substitution energy is given by:

$$\mathrm{E}_{sub} = \mathrm{E}_{\mathrm{Si_{n-1}TO_{2n}}(b)} + \mathrm{E}_{\mathrm{SiO_2}(q)} - n\mathrm{E}_{\mathrm{SiO_2}(b)} - \frac{1}{2}\mathrm{E}_{\mathrm{T_2O_3}(c)} - \frac{1}{2}\mathrm{E}_{\mathrm{O_2}(m)}. \tag{2}$$

where $\mathrm{E}_{\mathrm{Si_{n-1}TO_{2n}}(b)}$, $\mathrm{E}_{\mathrm{SiO_2}(q)}$, $\mathrm{E}_{\mathrm{O_2}(m)}$, $\mathrm{E}_{\mathrm{SiO_2}(b)}$ and $\mathrm{E}_{\mathrm{T_2O_3}(c)}$ are the total energies of the T-doped 2D zeolite, $\alpha-\mathrm{SiO_2}$ quartz, oxygen molecule, pure siliceous 2D zeolite and α-$\mathrm{T_2O_3}$, respectively. The calculated values for the substitution energy are displayed in Table 1. The corresponding substitution energy value for the B atom is negative whereas that one of Ga is positive. According to Eq. 2, a more negative substitution energy indicates greater thermodynamic stability. Therefore, our results show that the incorporation of B atom in the 2D zeolite model is exothermic and the insertion of Ga atom is endothermic. As mentioned in the introduction, Boscoboinik *et al*. [18, 19] have successfully synthesized Al-doped 2D zeolite. Hence, to quantify the experimental feasibility of B- and Ga-doped 2D zeolites, we can use the formation energy of Al-doped 2D zeolite which is calculated to be -9.74 eV using Eq. 2 as reference. It is found that the formation energy of the B-doped 2D zeolite is close to that of Al-doped 2D zeolite, whereas that one of Ga-doped zeolite is much higher. This indicates that B-doped 2D zeolite can be synthesized at room temperature whereas Ga-doped can be achieved using advance synthesis techniques such as high-temperature methods like solid-state diffusion and ion-exchange processes, or alternative techniques like atomic layer deposition (ALD) and chemical vapor deposition (CVD).

Having established the thermodynamic stability of the doped system, it is essential to investigate the electronic properties influenced by doping. Examing these properties offers deep understanding of how the dopant modifies the materials behaviour, which is crutial for potential applications.

3.2.3. Electronic properties

We also explored the influences of the trivalent B and Ga atoms on the electronic properties of the pure 2D zeolite model. Fig. 4 displays the DOS of the monodoped 2D zeolite model. We observed that the Fermi level is shifted towards the valence band maximum (VBM) which indicates that B and Ga atoms behave as $p-$type defects in the 2D zeolite system. This is because the insertion of the trivalent atoms induces an electronic hole in the valence band. Subsequently, we plotted the PDOS to get more understanding on the effects of the trivalent B and Ga atoms, more especially on the detailed contribution of the various orbitals of each element at the band edges. The obtained plots (Fig. 4) shows overlap between the O $2p$ states and the B (Ga) $2p$ ($4p$) states at the VBM, suggesting a strong interaction between them. On the conduction band (CB) side, it is found that the edge is predominantly contributed by the B (Ga) $2p$ ($4p$) and Si $3p$ orbitals. In addition, we also observed a state in the vicinity of the highest occupied states ($\sim$ 0.15 eV above the VBM). This state is originated from the hybridization of the p-orbitals of the Si and O atoms. To the best of our knowledge,

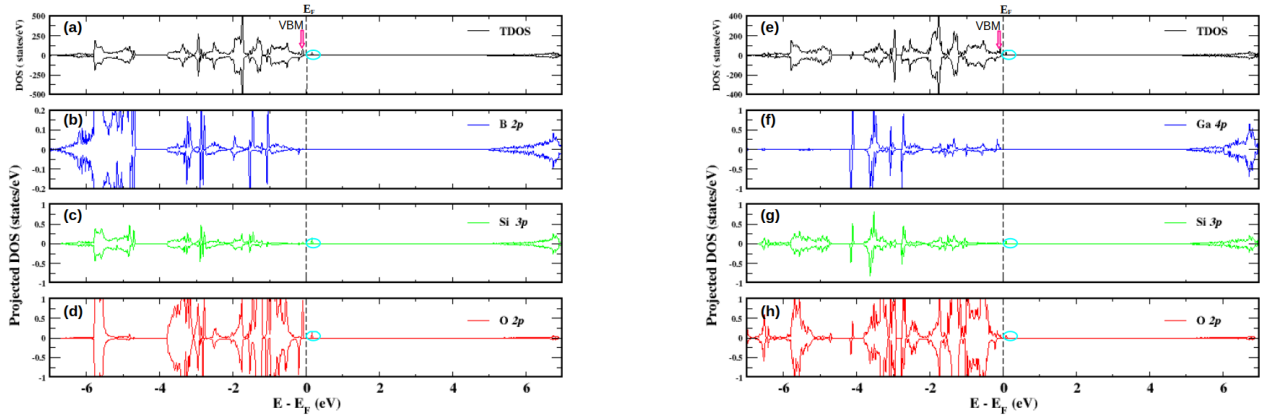

Figure 4: Total density of states (TDOS) and projected density of states (PDOS) of B-(left panel) and Ga-(right panel) doped 2D zeolite. The TDOS is shown as solid black line (a, e), while PDOS contributions from B (b) , Ga (f), Si (c, g) and O (d, h) are represented by colored curves. The Fermi level is set to 0 eV (dashed vertical line) for reference. A newly state at the vicinity of the VBM is circled in cyan. The shifting of the electronic states due to the B and Ga doping is observed, indicating modifications in the electronic structure and potential tuning of the 2D zeolite properties.

these results have not been reported in the bulk zeolites as the DOS analysis in zeolites is still scarce.

The substitution of Si with these trivalent atoms results in the formation of an anionic framework. During the synthesis the latter is balanced by the presence of extra-framework cations. In the next section, we will explore how these extra framework cations infuence the properties of the 2D zeolite.

3.3. Charge Compensation

In the experimental study by Boscoboinik *et al.* [18, 19], which proposed this bilayer silica as a 2D model for zeolite, the aluminosilicate 2D material were exposed to H_2O in order to see the formation of hydroxyl groups as observed in 3D zeolites. However, besides protons, various monovalent cations has been identify theoretically and experimentally as charge compensations in the bulk zeolites, influencing their applications. In the present study, we theoretically investigate the effect of proton as well as alkali metals such as Li, Na and K to compensate the charge due to the substitution of trivalent atoms.

3.3.1. Thermodynamic stability

We firstly determined the site preference of these monovalent cations. The crucial question is, do they prefer to be placed on the surface of the bilayer or as inner interstitials? To adress this question, three different adsorption sites were considered: the first site is on the surface at the middle of the hexagon (S_1) as shown in Fig 5a, the second (S_2) is on the surface but on top of the O bridging the T and Si atoms (see Fig 5b), and the last site (S_3) is inside the bilayer at the middle of the structure (see Fig 5c.)

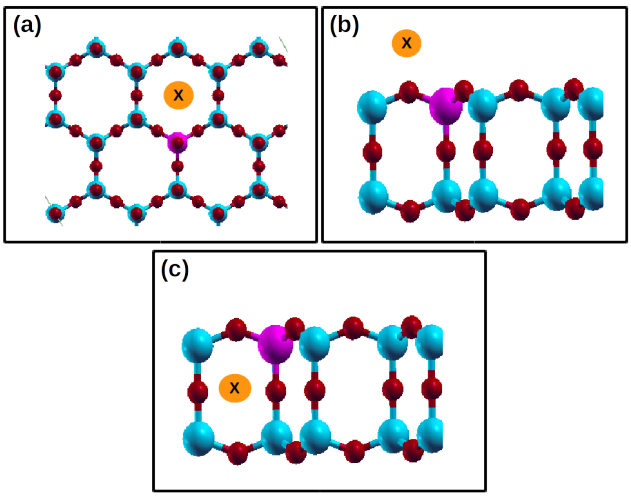

Figure 5: Location of the cations in the B and Ga-doped 2D zeolite studied in the present work.

From a thermodynamical point of view, the formation energy can be used to pre-select the experimental favorable structure and to define the synthesis conditions. According to Ref. [20], the formation energy of the protonated and alkali metal incorporated T-doped 2D zeolite can be calculated based on the fol-

Table 2: Calculated formation energy (eV) values for each alkali metal incorporated T-doped 2D zeolite (T = B, Ga) system.

	B				Ga			
	H	Li	Na	K	H	Li	Na	K
S_1	-14.53	-13.08	-13.15	-13.25	3.99	5.43	5.35	5.26
S_2	-14.53	-13.08	-13.14	-13.25	4.00	5.44	5.36	5.26
S_3	-14.50	-13.07	-13.15	-13.24	4.01	5.44	5.35	5.27

lowing chemical reaction:

$$n\mathrm{SiO_2}\ (b) + \frac{1}{2}\mathrm{T_2O_3}\ (c) + \frac{1}{2}\mathrm{M_2O}\ (af) \longrightarrow \mathrm{Si_{n-1}TMO_{2n}}\ (b) + \mathrm{SiO_2}\ (q)\ . \tag{3}$$

where T = (B, Ga), M = (H, Li, Na, K) and n is the number of tetrahedra in the system. The letters in between brackets have been defined in section 3.2.2, except af which indicates the antifluorite structure. According to this equation, the substitution energy is given by:

$$\mathrm{E}_{sub} = \mathrm{E}_{\mathrm{Si_{n-1}TMO_{2n}}(b)} + \mathrm{E}_{\mathrm{SiO_2}(q)} - n\mathrm{E}_{\mathrm{SiO_2}(b)} - \frac{1}{2}\mathrm{E}_{\mathrm{T_2O_3}(c)} - \frac{1}{2}\mathrm{E}_{\mathrm{M_2}O(af)}. \tag{4}$$

where $\mathrm{E}_{\mathrm{Si_{n-1}TMO_{2n}}(b)}$, $\mathrm{E}_{\mathrm{SiO_2}(q)}$, $\mathrm{E}_{\mathrm{M_2O}(af)}$, $\mathrm{E}_{\mathrm{SiO_2}(b)}$ and $\mathrm{E}_{\mathrm{T_2O_3}(c)}$ are the total energies of the protonated and alkali metal incorporated T-doped 2D zeolite, $\alpha-\mathrm{SiO_2}$ quartz, alkali metal oxide, pure siliceous 2D zeolite and α-$\mathrm{T_2O_3}$, respectively.

The obtained formation energy values are shown in Table 2. It is clearly seen that the values of the formation energy for each configuration do not differ significantly. It means that these configurations can co-exist during the synthesis of the 2D material system with charge compensation. For Na adsorption, the S_1 and S_3 structures became identical after atomic relaxation. In fact, the Na atom moved from the middle of the bilayer to the top of the hexagon surface. This is an interesting feature as the active sites are exposed at the surface, hence enhancing catalytic efficiency. This is one of the advantages of 2D materials in catalysis. In the remaining of this study, we are going to consider only the adsorption on the surface of the bilayer more especially at the middle of the six membered-ring (S_1) as this structure was observed experimentally in the case of Al doping, and also are slightly lower in formation energy (~ 10 meV less). Hydrogen has the lowest formation energy, making it the most favorable element for charge compensation. Among the alkali metals, K and Na have slightly lower formation energies (see Table 2), suggesting that group I element of the periodic table are best for charge compensation in 2D zeolite synthesis with a single trivalent atom substitution. These two elements were also found to be effective as charge balancing ions in the synthesis of B, Al and Ga incorporated SSZ-13 zeolites [11].

3.3.2. Structural properties

In this section, the geometry of the protonated and alkali metal incorporated B and Ga-doped 2D zeolites are described in details. The various relaxed structures for both cases are shown in Fig. 6. The key bond lengths and angles corresponding to each structure in Fig. 6 are depicted in Table 3.

Let's start the discussion with the relaxed structure of H incorporated B-doped 2D zeolite (H-B-2D zeolite) in Fig. 6a. The interesting characteristic of this system is the formation of a silanol group Si-OH and a trigonal BO_3 which is almost coplanar. This feature of H-B-2D zeolite has been observed experimentally via a solid state nuclear magnetic resonance (NMR) techniques in 3D zeolite [33], and also theoretically in various bulk zeolites [11, 12, 34, 35]. The interaction between these two groups is very weak due to the large distance between the silanol oxygen and the B atom which is approximately 2.50 Å.

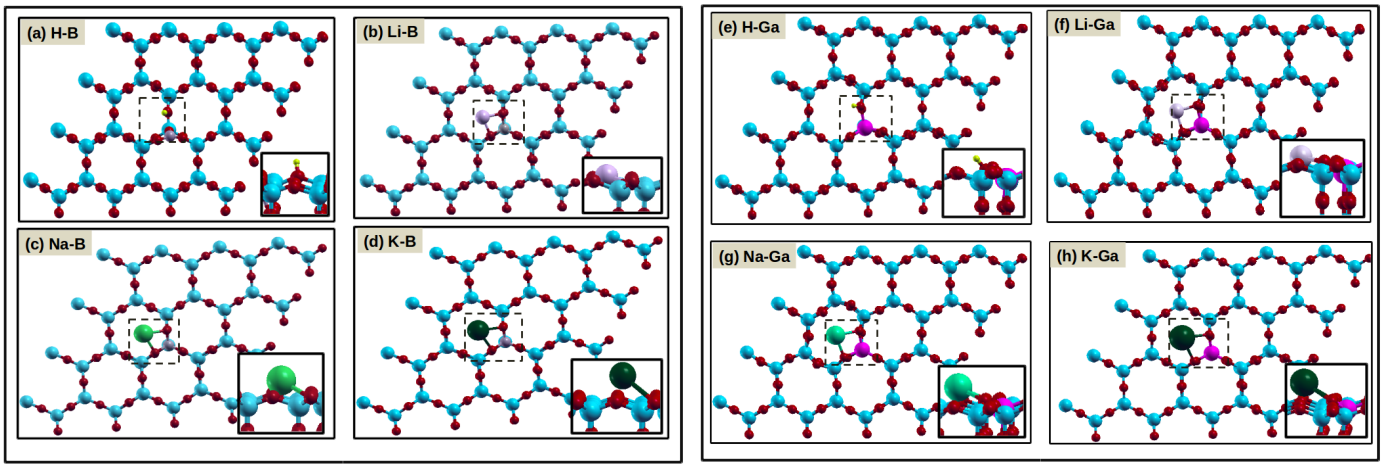

Figure 6: Relaxed structures of protonated and alkali metal incorporated (a, b, c, d) B-doped and (e, f, g, h) Ga-doped 2D zeolite. H, Li, Na, K, O, B, Ga and Si atoms are in yellow, purple, light green, dark green, red, grey, magenta and blue, respectively.

This bond distance is consistent with the value reported for bulk zeolites [11]. We also observed that the B-O bonds in the BO_3 structure are shorter compared to those of the tetrahedral B-site. The hydroxyl H−O bond length in the H-B-2D zeolite has a value of 0.97 Å which is found to be similar to the H−O bond length measured in the water molecule as well as in 3D zeolites such as H-B-SSZ-13, H-B-MTW, H-B-SOD, H-B-CHA, etc [11, 35].

In the case of alkali metal incorporated B-doped 2D zeolite, the alkali metal atoms were found to remain on top of the initial six membered ring, but they moved towards the B atom. They are coordinated with two bridging O atoms denoted by O_1 and O_2 with equal distance (first nearest neighbor). These results match the structural properties seen in 3D zeolites [11]. The geometry analysis of the relaxed structures presented in Figs. 6(a,b,c,d) reveals that the distances between the alkali metals and these nearest neighbor O atoms increase with the increase in element mass of the alkali adsorbed (see Table 3). In contrast, the change in B−O_1 and B−O_2 bond length values decrease with the increase in atomic radius of the alkali metal, suggesting that heavier alkali elements do not significantly affect the intra-framework bonds compared to the lighter ones.

We noticed that B−O_1 and B−O_2 bond lengths are larger

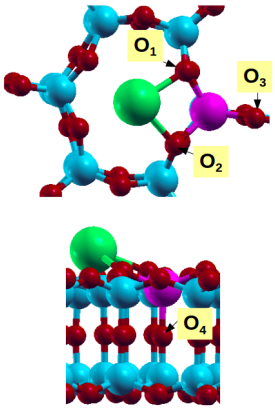

Figure 7: Numerotation of the oxygens surrounding the T atom

compared to the B−O bond in B-doped 2D zeolite for all structures. This may be due to the bond weakening effect caused by the introduction of the alkali metal in the framework. Due to this extension of B−O_1 and B−O_2 bond lengths, the other 2 bonds of the tetrahedra namely B−O_3 (one of the bond on surface not coordinated to the alkali metal) and B−O_4 (the axial bond) are slightly shorter compared to the B−O bond in B-doped 2D zeolite. We also observed that the vertical height of the alkali metals with respect to the surface of the bilayer depends on the atomic radius of the alkali element (K > Na > Li). This trend is in line with the observation in alkali metal

Table 3: Relevant bond lengths in Å for each alkali metal incorporated T-doped 2D zeolite (T = B, Ga) system.

	T = B				T = Ga			
Data	H	Li	Na	K	H	Li	Na	K
X-T	2.99	2.52	3.02	3.41	2.61	2.77	3.15	3.56
X-O1	0.97	1.93	2.37	2.74	0.97	1.99	2.35	2.76
X-O2	2.94	1.93	2.37	2.74	2.91	1.98	2.35	2.75
T-O1	2.54	1.56	1.53	1.53	1.82	1.92	1.90	1.88
T-O2	1.39	1.56	1.53	1.52	2.08	1.92	1.90	1.87
T-O3	1.39	1.44	1.45	1.46	1.82	1.82	1.82	1.83
T-O4	1.38	1.45	1.46	1.47	1.85	1.83	1.84	1.84

adsorbed on other 2D materials [36]. Although the structural analysis reveals some changes on the different bond lengths, a significant deformation of the hexagonal feature of the bilayer material is not observed, indicating that the alkali metals are good candidates for charge compensation in the B-doped 2D zeolite model (known as boralite in the 3D zeolite).

Fig. 6(f,g,h) show the relaxed structures of the alkali metal adsorbed on the surface of Ga-doped 2D zeolite. They show almost the same structural behavior as alkali metal adsorbed on the surface of the B-doped 2D zeolite. However, since Ga atom has larger atomic radius compared to B atom as well as Si atom, the values of the bond lengths for alkali metal adsorption (as seen in Table. 3) are higher compared to the pristine and B-doped zeolite. In the case of protonated Ga-doped 2D zeolite (H-Ga-2D zeolite), it can be seen from Fig. 6e that it is tetra-coordinated with Ga$-O_1$, Ga$-O_2$, Ga$-O_3$, Ga$-O_4$ distance values of 1.80, 2.08, 1.82, 1.82 Å, respectively. Ga$-O_2$ is clearly elongated compared to the other three Ga$-$O bonds due to the presence of the H$-$O bond that weakens the bond between the Ga and the bridging O atom. These results are in line with the DFT results of H-Ga-SSZ-13 zeolites [11]. The presence of the tetrahedral Ga in 3D zeolites was also experimentally revealed by NMR spectra. [37, 38] To the best of our knowledge, no experimental study has been reported on controlling the incorporation of trivalent B and Ga in the 2D zeolite model using different alkali metal ions. Our calculations provide a new option to selectively synthesize B- and Ga-doped 2D zeolite using H, Li, Na and K ions, which need to be confirmed by experiments.

Generally, the electronic properties study provides important information regarding the chemical and physical properties of a specific material. It can also give insight into the appropriate industrial applications of the compound. In the following section, the electronic properties of various systems are analyzed.

3.3.3. Electronic properties

In this section, the density of states (DOS) of the protonated and alkali metal incorporated B and Ga-doped 2D zeolite are ploted and inspected thoroughly in order to investigate their electronic properties. Fig. 8 presents the total and partial DOS of the Li-, Na-, K-B-doped 2D zeolite. These are used as examples since a similar trend is expected for both cases B- and Ga-doped 2D zeolite. The band edges characteristics are primarily studied in order to identify which orbitals of the neighboring atoms overlap and also to predict the nature of chemical bonding. As shown in Fig. 8, the DOS peak of B-doped 2D zeolite is weaker than that of H-B-doped 2D zeolite because the O $2p$ orbital of the former is more populated than the latter. We also observed that the position of the bilayer Fermi level affected by the introduction of trivalent atom, is now shifted again within the band gap. This indicates that H atom induces a red-shift into the system. Comparing the DOS of the H-B-2D zeolite (Fig. 8a) with that of B-doped and pristine 2D zeolite (Fig. 4

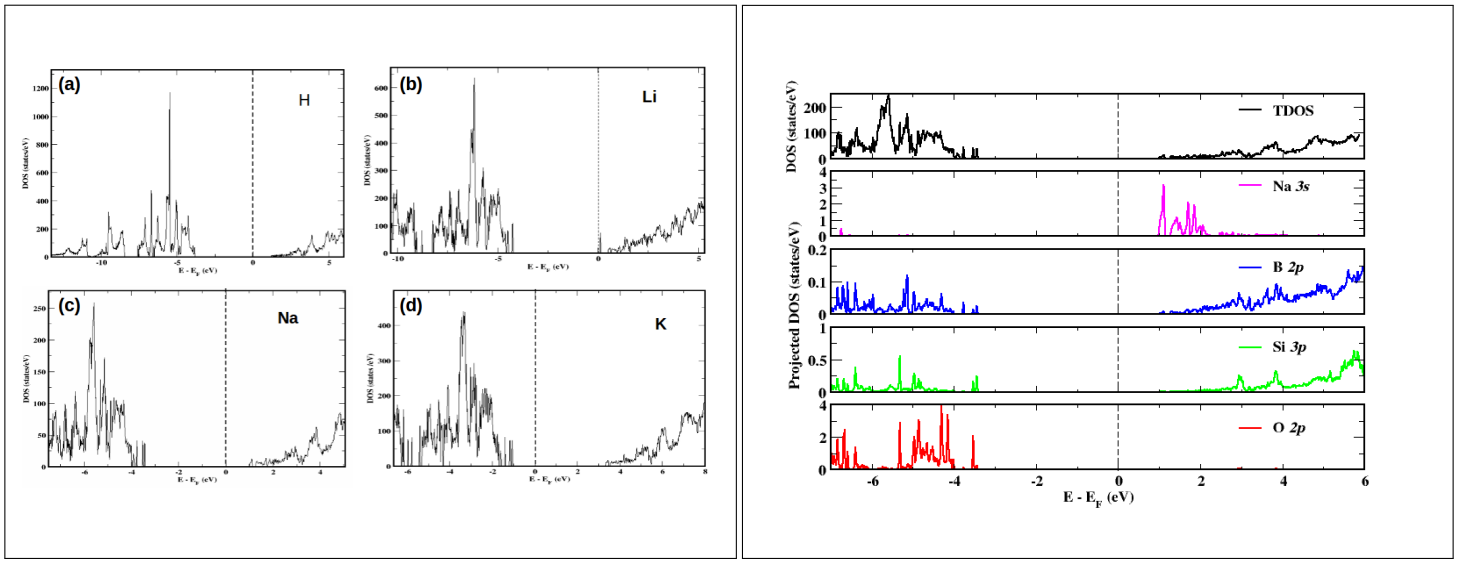

Figure 8: Left: Total density of states (TDOS) of (a) H, (b) Li, (c) Na, (d) K incorporated B-doped 2D zeolite, highlighting the impact of different cations on the electronic structure. Right: Partial density of states (PDOS) of Na-B-2D zeolite (considered as a typical model) to illustrate the cation specific electronic contributions. The black line corresponds to the TDOS plot. Magenta, blue, green and red lines indicate the *s* orbital of Na, *p* orbital of B, *p* orbital of the Si and *p* orbital of O atoms, respectively.

and Fig. 2 respectively) reveals that H-B-2D zeolite closely resembles the DOS shape of the pristine. The proton makes no significant contributions at the bond edges, with the main contributions coming from the zeolite framework.

In contrast to protonated B-doped 2D zeolite, the introduction of alkali metal into the B-doped 2D zeolite alters the band gap of the system (see Fig. 8b,c,d). On the CB side, the *s* orbitals of the Na, Li and K adatoms are shifted to the lower energy region compared to those of zeolite framework. This can be seen in Fig. 8b which shows the PDOS of Na-B-2D zeolite. This was observed in the case of lamellar zeolites of ZSM-5 type with Na as charge compensation. These materials were reported to offer two distinct advantages over mesoporous zeolites as they preserve precise size selectivity while minimizing the diffusion pathway through the micropores between the lamellae [39]. Moreover, the DOS plots in Fig. 8b,c,d show the formation of extra gap states near the VBM, mainly originated from the hybridization of 2*p* orbitals of the B atom and the neighboring O atoms. Accordingly, strong covalent interactions exist between B(Ga) and O atoms. These modifications around the band edges cause a shortening of the band gap of the systems. Usually, the reactivity of a material is associated with the position of the top of the valence band (VBM) and the bottom of conduction band (CBM), in another words the smaller the band gap is (or absent) the more reactive the system is. These results suggest that the alkali metal could obviously increase the reducibility of the band gap of the bilayer system. Furthermore, the alkali metal *s* state has no visible contribution to the VB, suggesting that they are highly ionised.

As shown in the previous paragraph, the proton and the alkali metal behaves differently, let's see if it reflects on the nature of bonding. It can be identified by investigating the electron distribution in the system. In the present study, to predict the type of chemical bonding between the alkali metal and the 2D ze-

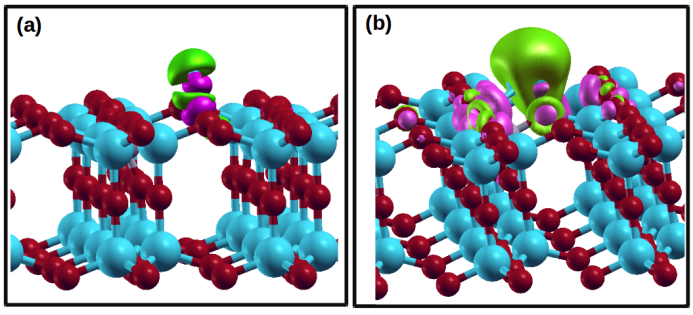

Figure 9: Charge density difference in a (a) protonated and (b) alkali metal incorporated in a 2D zeolite with one Si substituted by trivalent atom.

olite framework, charge density differences are calculated and depicted in Fig. 9. For the protonated B-2D zeolite model, we observe that the charges are accumulated in the bond between the O and H atoms (see Fig. 9a) indicating they are covalently bonded. For the case of adsorption of alkali metal on the B-2D doped zeolite, the depletion region is mainly located at the alkali metal, while the accumulated charge is found around the alkali neighboring O atoms (see Fig. 9b). This reveals the presence of ionic bond between the alkali metal and the O atoms. The difference in bonding behavior between the proton and alkali metals to the 2D zeolite framework is expected to originate from the dissimilar electronegativity. The large difference in electronegativity between O and alkali metal is responsible for charge transfer among different atoms resulting in ionic bond nature, while the small electronegativity difference between H and O atoms results in charge sharing and is responsible for covalent bond nature.

3.3.4. Acid site strength for T-doped 2D zeolite

From the stability analysis, we found that H is the most stable cation to balance the unpaired electron created by the introduction of trivalent atoms in the 2D zeolite model. Furthermore, zeolites are popularly used for acid catalysis in the industry. In this section, we particularly evaluate the acid strength of the Brønsted acid site of H-B-, and H-Ga-doped 2D zeolite. One of the most direct computational approach to predict the acidity and reactivity of bulk zeolites is the evaluation of the proton affinity (PA) [40, 12]. PA has been reported to reproduce qualitatively the experimental results on the relative acidity strength of bulk zeolites such as in the case of ZSM-5 substituted with B, Al, Ga and Fe. [40, 12] It is defined as the energy required to remove a proton from the zeolitic neutral structure and leaving an anionic system.

$$\mathrm{ZeoOH} \longrightarrow \mathrm{ZeoO^-} + \mathrm{H^+}. \tag{5}$$

PA is then calculated as the energy difference between $\mathrm{ZeoO^-}$ and ZeoOH. The higher the PA, the poorer proton donor the system is and, in consequence, the lower the Brønsted acidity is [40].

In our study, a value of 1.408 and 1.025 eV is obtained for H-B- and H-Ga-doped 2D zeolite respectively. The calculated PA of a B-doped is higher than Ga-doped 2D zeolite. This indicates the low acid strength of B-doped 2D zeolite model. The low acid strength of B-doped zeolite could be due to the trigonal coordination of B-doped zeolite upon the adsorption of H atom [40]. This trend is similar to what is observed in various bulk zeolites. [11, 12, 40]. Our finding suggests that B-doped zeolite can be beneficial for selective catalytic reactions like hydrocarbon cracking, isomerization, and aromatization.

4. Conclusion

Computational studies on the properties of trivalent atoms such as B and Ga containing 2D zeolite, having proton and alkali metal as charge compensation, have been performed using DFT approaches. The relative synthesis difficulty level of the insertion of B and Ga atoms was firstly evaluated by calculating the substitution energy. Incorporating B atom in the 2D system is found to be less difficult than Ga atom. The electronic properties studies show that these trivalent atoms are sources of *p*-type conductivity in the silica bilayer due to the one electron removal. The present study also aims to identify the appropriate charge compensation during synthesis to mimic the experimental scenario observed in the 3D zeolite. The structural studies showed that H-, Li-, Na- and K-B and Ga-doped 2D zeolite are tetra-coordinated except H-B-2D zeolite, in which three-fold coordination for B is favorable. H has the lowest formation energy and among the alkali metals, K and Na were found to be the most suitable charge balanced. It was also found that the introduction of alkali metals induces states near the band edges reducing the band gap of the system. The position of these states depend on the atomic radius of the foreign atom. This indicate that the introduction of alkali metal enhances the reactivity of the bilayer system. Charge analysis revealed that the H atom is covalently bonded to the O atom while the alkali metals have ionic bond due to the large electronegativity difference. These results show the formation of Brønsted acid site for the protonated 2D zeolite, similar finding to those of 3D zeolites

and the Al-doped 2D zeolite. Furthermore, the strength of this Brønsted acid site was qualitatively evaluated and compared based on the calculated proton affinity. The results showed low acidity of B-doped 2D zeolite model compared to Ga-doped, a similar trend to that of bulk zeolite. In summary, the present study provides valuable insights into the stability and electronic properties of B and Ga-doped 2D zeolites, offering a foundation for their potential applications in catalysis such as the isomerization, and selective adsorption processes. Our results contribute to a deeper understanding of their electronic structure, which could inform future experimental and theoretical investigations. However, the synthesis of these materials may present challenges, particularly in maintaining structural integrity and achieving desired electronic properties under practical conditions. Addressing these limitations through advanced synthesis techniques and further computational studies will be essential for realizing their full potential in technological applications

Acknowledgment

The authors acknowledge Johnson Matthey for financial support, the Center for High Performance Computing (CHPC), South Africa for computational resources. NC acknowledges support from Prof Mark Hybertsen at the Centre for Functional Nanomaterials, Brookhaven National Laboratory for useful discussions and suggestions.

References

[1] H. Soscún, O. Castellano, J. Hernandez, F. Arrieta, Y. Bermúdez, A. Hinchliffe, M. R. Brussin, M. Sanchez, A. Sierraalta, F. Ruette, An ab initio and dft study of the interaction between ethanethiol and zeolites, Journal of Molecular Catalysis A: Chemical 278 (1-2) (2007) 165–172.

[2] C. E. Hernandez-Tamargo, A. Roldan, N. H. de Leeuw, Density functional theory study of the zeolite-mediated tautomerization of phenol and catechol, Molecular Catalysis 433 (2017) 334–345.

[3] B. D. Montejo-Valencia, Y. J. Pagàn-Torres, M. M. Martínez-Iñesta, M. C. Curet-Arana, Density functional theory (dft) study to unravel the catalytic properties of M-exchanged MFI,(M= Be, Co, Cu, Mg, Mn, Zn) for the conversion of methane and carbon dioxide to acetic acid, ACS Catalysis 7 (10) (2017) 6719–6728.

[4] M. E. Davis, R. F. Lobo, Zeolite and molecular sieve synthesis, Chemistry of Materials 4 (4) (1992) 756–768.

[5] T. R. Gaffney, Porous solids for air separation, Current Opinion in Solid State and Materials Science 1 (1) (1996) 69–75.

[6] N. Moreno, X. Querol, C. Ayora, C. F. Pereira, M. Janssen-Jurkovicová, Utilization of zeolites synthesized from coal fly ash for the purification of acid mine waters, Environmental science & technology 35 (17) (2001) 3526–3534.

[7] S. Ouki, M. Kavannagh, Treatment of metals-contaminated wastewaters by use of natural zeolites, Water Science and Technology 39 (10-11) (1999) 115–122.

[8] K. S. Walton, M. B. Abney, M. Douglas LeVan, CO_2 adsorption in Y and X zeolites modified by alkali metal cation exchange, Microporous and Mesoporous Materials 91 (1) (2006) 78–84.

[9] B. Civalleri, A. M. Ferrari, M. Llunell, R. Orlando, M. Merawa, P. Ugliengo, Cation selectivity in alkali-exchanged chabazite: An ab initio periodic study, Chemistry of materials 15 (21) (2003) 3996–4004.

[10] C. T. Chu, C. D. Chang, Isomorphous substitution in zeolite frameworks. 1. acidity of surface hydroxyls in B-,Fe-,Ga-, and Al-ZSM-5, The Journal of Physical Chemistry 89 (9) (1985) 1569–1571.

[11] C. Wen, L. Geng, L. Han, J. Wang, L. Chang, G. Feng, D. Kong, J. Liu, A comparative first principles study on trivalent ion incorporated SSZ-13 zeolites, Physical Chemistry Chemical Physics 17 (44) (2015) 29586–29596.

[12] S. Yuan, J. Wang, Y. Li, H. Jiao, Brønsted acidity of isomorphously substituted ZSM-5 by B, Al, Ga, and Fe. density functional investigations, The Journal of Physical Chemistry A 106 (35) (2002) 8167–8172.

[13] C. V. Hoang, T. M. Nguyen, D. L. T. Nguyen, K. N. Dinh, H. T. Dang, Q. V. Le, Recent advances in nanoengineering 2D metal-based materials for electrocatalytic conversion of carbon dioxide into fuels and value-added products, Fuel 343 (2023) 127873.

[14] J. Mao, P. Liu, C. Du, D. Liang, J. Yan, W. Song, Tailoring 2D MoS_2 heterointerfaces for promising oxygen reduction reaction electrocatalysis, Journal of Materials Chemistry A 7 (15) (2019) 8785–8789.

[15] X. Yin, Y. Hua, Z. Gao, Two-dimensional materials for high-performance oxygen evolution reaction: Fundamentals, recent progress, and improving strategies, Renewables 1 (2) (2023) 190–226.

[16] M. Choi, K. Na, J. Kim, Y. Sakamoto, O. Terasaki, R. Ryoo, Stable single-unit-cell nanosheets of zeolite MFI as active and long-lived catalysts, Nature 461 (7261) (2009) 246–249.

[17] R. Wei, H. Yang, J. A. Scott, K.-F. Aguey-Zinsou, D. Zhang, 2d versus 3d MFI zeolite: The effect of si/al ratio on the accessibility of acid sites and catalytic performance, Materials today chemistry 8 (2018) 1–12.

[18] J. A. Boscoboinik, S. Shaikhutdinov, Exploring zeolite chemistry with the tools of surface science: challenges, opportunities, and limitations, Catalysis letters 144 (12) (2014) 1987–1995.

[19] J. A. Boscoboinik, X. Yu, B. Yang, F. D. Fischer, R. Włodarczyk, M. Sierka, S. Shaikhutdinov, J. Sauer, H.-J. Freund, Modeling zeo-

lites with metal-supported two-dimensional aluminosilicate films, Angewandte Chemie International Edition 51 (24) (2012) 6005–6008.

[20] A. Malashevich, S. Ismail-Beigi, E. I. Altman, Directing the structure of two-dimensional silica and silicates, The Journal of Physical Chemistry C 120 (47) (2016) 26770–26781.

[21] P. Schlexer, L. Giordano, G. Pacchioni, Adsorption of Li, Na, K, and Mg atoms on amorphous and crystalline silica bilayers on Ru (0001): A DFT study, The Journal of Physical Chemistry C 118 (29) (2014) 15884–15891.

[22] P. Giannozzi, S. Baroni, N. Bonini, M. Calandra, R. Car, C. Cavazzoni, D. Ceresoli, G. L. Chiarotti, M. Cococcioni, I. Dabo, et al., Quantum espresso: a modular and open-source software project for quantum simulations of materials, Journal of physics: Condensed matter 21 (39) (2009) 395502.

[23] P. Giannozzi, O. Andreussi, T. Brumme, O. Bunau, M. B. Nardelli, M. Calandra, R. Car, C. Cavazzoni, D. Ceresoli, M. Cococcioni, et al., Advanced capabilities for materials modelling with quantum espresso, Journal of Physics: Condensed Matter 29 (46) (2017) 465901.

[24] J. P. Perdew, K. Burke, M. Ernzerhof, Generalized gradient approximation made simple, Phys. Rev. Lett. 77 (18) (1996) 3865.

[25] P. E. Blöchl, Projector augmented-wave method, Phys. Rev. B 50 (24) (1994) 17953.

[26] T. Thonhauser, S. Zuluaga, C. Arter, K. Berland, E. Schröder, P. Hyldgaard, Spin signature of nonlocal correlation binding in metal-organic frameworks, Physical review letters 115 (13) (2015) 136402.

[27] T. Thonhauser, V. R. Cooper, S. Li, A. Puzder, P. Hyldgaard, D. C. Langreth, Van der waals density functional: Self-consistent potential and the nature of the van der waals bond, Phys. Rev. B 76 (2007) 125112.

[28] K. Berland, V. R. Cooper, K. Lee, E. Schröder, T. Thonhauser, P. Hyldgaard, B. I. Lundqvist, van der Waals forces in density functional theory: a review of the vdw-DF method, Reports on Progress in Physics 78 (6) (2015) 066501.

[29] M.-J. Díaz-Cabañas, P. A. Barrett, Synthesis and structure of pure SiO_2 chabazite: the SiO_2 polymorph with the lowest framework density, Chemical Communications (17) (1998) 1881–1882.

[30] E. I. Altman, Group III phosphates as two-dimensional van der waals materials, The physical of Chemistry C 121 (14) (2017) 16328–16341.

[31] G. Calzaferri, C. Leiggener, S. Glaus, The electronic structure of Cu^+, Ag^+, and Au^+ zeolites, Chemical Society Reviews 32 (1) (2003) 29–37.

[32] C. E. Hernandez-Tamargo, A. Roldan, N. H. de Leeuw, A density functional theory study of the structure of pure-silica and aluminium-substituted MFI nanosheets, Journal of Solid State Chemistry 237 (2016) 192–203.

[33] S.-J. Hwang, C.-Y. Chen, S. I. Zones, Boron sites in borosilicate zeolites at various stages of hydration studied by solid state nmr spectroscopy, The Journal of Physical Chemistry B 108 (48) (2004) 18535–18546.

[34] F. Trudu, G. Tabacchi, A. Gamba, E. Fois, First principles studies on boron sites in zeolites, The Journal of Physical Chemistry A 111 (45) (2007) 11626–11637.

[35] Y. Wang, D. Zhou, G. Yang, S. Miao, X. Liu, X. Bao, A DFT study on isomorphously substituted MCM-22 zeolite, The Journal of Physical Chemistry A 108 (32) (2004) 6730–6734.

[36] D. Er, J. Li, M. Naguib, Y. Gogotsi, V. B. Shenoy, Ti_3C_2 mxene as a high capacity electrode material for metal (Li, Na, K, Ca) ion batteries, ACS applied materials & interfaces 6 (14) (2014) 11173–11179.

[37] M. Yabushita, M. Yoshida, F. Muto, M. Horie, Y. Kunitake, T. Nishitoba, S. Maki, K. Kanie, T. Yokoi, A. Muramatsu, Hydrothermal synthesis of ga-substituted MFI zeolites via a mechanochemical process and their catalytic activity for methane transformation, Molecular Catalysis 478 (2019) 110579.

[38] H. K. C. Timken, E. Oldfield, Solid-state gallium-69 and gallium-71 nuclear magnetic resonance spectroscopic studies of gallium analog zeolites and related systems, Journal of the American Chemical Society 109 (25) (1987) 7669–7673.

[39] J. Antúnez-García, R. I. Yocupicio-Gaxiola, A. R. Serrato, V. Petranovskii, F. N. Murrieta-Rico, M. G. Shelyapina, S. Fuentes-Moyado, A theoretical study of the effect of exchange cations in surface of ZSM-5 lamellar zeolites, Journal of Solid State Chemistry 317 (2023) 123725.

[40] A. Chatterjee, T. Iwasaki, T. Ebina, A. Miyamoto, Density functional study for estimating brønsted acid site strength in isomorphously substituted ZSM-5, Microporous and mesoporous materials 21 (4-6) (1998) 421–428.